Particle-core analysis of mismatched beams in a periodic focusing channel

Masanori Ikegami
Proton Accelerator Laboratory, Japan Atomic Energy Research Institute, Tokai-mura, Naka-gun, Ibaraki-ken 319-1195, Japan
(Received 31 August 1998)

A method is derived for applying particle-core analysis to mismatched beams in a periodic focusing channel. By carefully choosing the parameters to yield a favorable core frequency, a Poincaré surface of section plot is obtained. The plots for a periodic solenoid channel exhibit a striking resemblance to those in continuous focusing cases, while those for an alternating-gradient channel exhibit a strong chaoticity which is not seen in the corresponding continuous focusing situation. Only the breathing mode oscillation of a core has been considered in solenoid focusing cases. On the other hand, the quadrupole mode oscillation of a core has also been considered in the case of an alternating gradient channel. We examine the effects of both modes on the test particle stability, and find that the quadrupole mode oscillation can also drive the particle-core resonance and cause beam halo formation. The halo extent is also examined. The maximum halo width is found to be about twice as large as the maximum core width in breathing oscillation cases in both periodic solenoid and alternating-gradient channels. In quadrupole oscillation cases, the halo width exhibits density dependence, and ranges from 1.2 to 2 times the maximum core width. These results give us a practical criterion to determine the bore radius in designing high-intensity accelerators. [S1063-651X(99)06502-2]

PACS number(s): 41.75.−i, 29.27.Bd, 52.25.Wz

I. INTRODUCTION

In recent years, it has been proposed to use high-intensity and high-power ion accelerators as a driver for a spallation neutron source, production of tritium, transmutation of nuclear waste, etc. [1]. In designing these next-generation accelerators, it is extremely important to understand clearly space-charge-induced phenomena, such as structure-driven resonance, charge redistribution, equipartitioning, and beam halo formation. It is especially essential to understand fully the beam halo formation mechanism, because a small fraction of beam loss causes serious radioactivation of the accelerator structure and prevents hands-on maintenance.

From this point of view, halo formation in intense ion beams has been studied extensively in both theoretical and numerical ways. In these studies, the so-called *particle-core model* [2,3] has frequently been used. In this model, we usually consider a beam propagating in a continuous focusing channel, and assume that its core has a Kapchinskij-Vladimirskij (KV) distribution [4]. Initial beam-size mismatch induces the oscillation of a core. Test particles initially located outside the core execute betatron oscillation under the influence of the nonlinear space-charge field induced by the oscillating core. We examine the time evolution of test particles, assuming that the core oscillation is not influenced by the motion of these test particles. The tune of the betatron oscillation is amplitude dependent due to the nonlinearity of the space-charge field. Therefore, a test particle is trapped at certain amplitude by the 2:1 resonance between core and test particle oscillation. Test particles with certain initial conditions gain excess energy through the resonance and form halos. When the beam density and the degree of mismatch are higher than certain thresholds, resonance overlap and chaos [5] are observed in test particle motion. The chaosity is thought to play a key role in enhancing the chance for the particles initially located just outside the core to be trapped by the resonance. A map of trajectories followed by test particles placed at given starting positions can be obtained by the Poincaré surface of section technique for this simple model. This non-self-consistent test particle method gives us a clear insight into the halo formation process, while it is difficult to use it to explore the transport dynamics. That is, it is difficult to examine with this model whether the particles initially located inside a core can escape from the core and form halos.

An approach that also allows the transport dynamics to be investigated in the beam-halo study is a self-consistent simulation using macroparticles. In self-consistent simulation studies of continuously focused beams, features such as the separatrix and fixed point locations are found to be in good agreement with those obtained with the particle-core model [6].

Halo properties in periodically focused cases were also studied self-consistently. In that study, a close resemblance to the continuous focusing cases was found for a periodic solenoid channel, unless instability due to structure-driven resonance is induced [7]. Though the role of the particle-core resonance in a periodic focusing situation can be directly investigated by applying the particle-core model, very few attempts have been made to apply the model to mismatched cases except for the pioneering work performed by Lagniel [8]. This is mainly due to the difficulty in finding the fundamental frequency of the system. In the particle-core analysis, the Poincaré mapping technique is an essential tool to examine the stability properties of test particles, and we need to know the fundamental frequency of the system to use this technique. It is generally difficult to know the fundamental frequency in periodic focusing cases because there are two sources of periodicity, namely, the external focusing field periodicity and that due to initial beam-size mismatch. In fact, the solution of the envelope equation itself is known to show very complicated features including parametric resonance and chaos [9]. The effect of the unstable behavior of the envelope on halo formation is also an interesting subject.

However, it seems to be reasonable to restrict our interest to cases where core oscillation is stable, taking into account the resemblance mentioned above and the fact that the envelope is known to be stable with a reasonable choice of parameters. From that point of view, we have tried to obtain the fundamental frequency of stable core oscillation, and apply the particle-core model to mismatched beams in a periodic focusing channel.

In Sec. II, we present the method of applying the particle-core model to mismatched beams in a periodic channel. Then we apply the method to mismatched beams in a periodic solenoid channel. In this case, we assume that the beam and external focusing field have an axial symmetry, and, hence, only the breathing mode oscillation can be excited. In Sec. III, we apply the same method to mismatched beams in an alternating-gradient focusing channel. As a test channel, we employ a FODO channel with a 50% filling factor, each cell of which consists of a focusing quarupole magnet and a defocusing quadrupole magnet of equal strength. In this case, the beam and external focusing field have no axial symmetry, and, hence, both the breathing and quadrupole mode oscillation can be excited. In Sec. IV, we estimate the maximum halo extent in periodic focusing channels. After discussions, a summary is given in Sec. V. In the present study, we will restrict our treatment to test particles with zero angular momentum and an unbunched core with the KV distribution.

II. AXIALLY SYMMETRIC CHANNEL

A. Numerical method

Assuming axial symmetry of the beam and an external focusing field, the time evolution of a beam envelope is governed by the envelope equation

$$\frac{d^2R_b}{ds^2}+\kappa(s)R_b-\frac{K}{R_b}-\frac{\varepsilon^2}{R_b^3}=0, \tag{1}$$

where R_b is the beam radius, $\kappa(s)$ is the periodic function representing the external focusing field strength, K is the generalized perveance, ε is the rms emittance of the beam, and the independent variable s is the distance measured along the beam line. Then we transform the envelope equation to a dimensionless form using the following dimensionless parameters and variables: $\tau=s/S$ for the independent variable, $\vartheta(\tau)=S^2\kappa(s)$ for the dimensionless focusing strength function, $\Gamma=KS/\varepsilon$ for the scaled space-charge perveance, and $R=R_b/\sqrt{\varepsilon S}$ for the scaled beam radius, with S the length of a focusing cell. In terms of new variables, Eq. (1) becomes

$$\frac{d^2R}{d\tau^2}+\vartheta(\tau)R-\frac{\Gamma}{R}-\frac{1}{R^3}=0. \tag{2}$$

The function $\vartheta(\tau)$ is related to the zero-current phase advance σ_0, and Γ is related to the tune depression η, that is, the ratio of the space-charge depressed phase advance to the zero-current phase advance. The matched solution R_0 of Eq. (2) can be obtained with the help of an optimization code. For later reference, here we introduce a mismatch parameter which is a measure of the degree of initial beam-size mismatch, and defined as $M=[R(0)-R_0(0)]/R_0(0)$. It should be noted that $R_0(0)$ corresponds to the maximum radius of a matched beam since the origin of the coordinate τ is located at the center of a focusing solenoid.

With the use of the smooth approximation, we can move to the corresponding constant focusing situation simply putting $\vartheta(\tau)=\sigma_0^2$ [10]. Therefore, Eq. (2) can be rewritten in the smooth approximation as

$$\frac{d^2R_s}{d\tau^2}+\sigma_0^2R_s-\frac{\Gamma}{R_s}-\frac{1}{R_s^3}=0, \tag{3}$$

where R_s is the scaled beam radius in the approximation. The equilibrium solution of Eq. (3) is given by $R_s^0=1/\sqrt{\sigma}$, which corresponds to the matched radius for the equivalent continuous focusing channel. Here we introduce a mismatch parameter which is defined, in an analogous way with periodic cases, as $M_s=[R_s(0)-R_s^0]/R_s^0$.

In weakly mismatched cases, the phase advance of the breathing mode oscillation of the envelope can be approximated by

$$\sigma_m=\sqrt{2(1+\eta^2)+\tfrac{1}{2}(1+9\eta^2)M_s^2}\,\sigma_0, \tag{4}$$

where we use a combination of a simple perturbation method and an averaging method [11]. Note here that only the breathing mode oscillation can be excited in this case because of the assumed axial symmetry of the beam and external focusing field.

Here we assume that the oscillation of a core can be approximated by a simple composition of two oscillation modes: one is excited by the initial beam-size mismatch (*mismatch mode*), and the other is excited by the periodic nature of a focusing structure (*structure mode*). Based on the smooth-approximation analysis above, the phase advance of the mismatch mode is expected to be σ_m. On the other hand, the fundamental period of the structure mode is apparently synchronized with the focusing structure. Thus, it is obvious that if $\sigma_m/2\pi$ is a rational number; that is, $\sigma_m/2\pi$ can be expressed by two relatively prime integers m and n as $\sigma_m/2\pi=n/m$, the mismatched envelope is exactly periodic in τ with the period of m [12]. Note here that, recalling Eq. (4), we can make $\sigma_m/2\pi$ rational by choosing appropriate values for η and M_s. We can easily obtain a Poincaré surface of section plot in such cases by plotting test particle locations every m focusing periods. That is our strategy to apply the particle-core method to mismatched beams in a periodic channel.

Finally, we write down the equation of motion for a test particle. Assuming that the core has a KV distribution and test particles have no angular momentum, the equation of motion in terms of the dimensionless variables is given by

$$\frac{d^2x}{d\tau^2}+\vartheta(\tau)x-\frac{\Gamma}{R^2}x=0 \quad (|x|\leqslant R) \tag{5}$$

and

$$\frac{d^2x}{d\tau^2}+\vartheta(\tau)x-\frac{\Gamma}{x}=0 \quad (|x|>R). \tag{6}$$

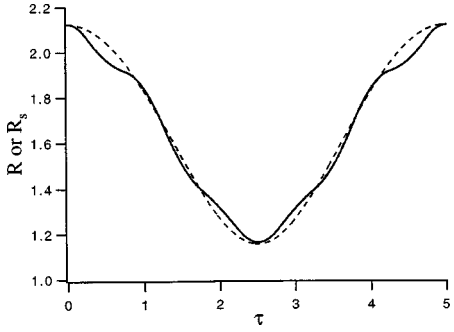

FIG. 1. Time evolution of the scaled beam envelope in a periodic solenoid channel. The parameters are set to $\sigma_0=45°$, $\eta=0.5$, and $M=0.3$ to yield $\sigma_m=72°$. The solid line represents the scaled beam radius obtained by numerically solving Eq. (2), while the broken line represents the solution for the corresponding continuous channel.

Numerically integrating Eqs. (2), (5) and (6), we can obtain the time evolution of the test particles. In the integration, the fourth-order symplectic integration algorithm [13] is employed.

B. Numerical results

Here let us show an example in which we consider a periodically interrupted solenoid channel having $\sigma_0=45°$ and a 50% filling factor. The beam parameters are set to be $\eta=0.5$ and $M=0.3$. These parameters are determined to yield $\sigma_m=360/5=72°$ by Eq. (4) with the help of an optimization code [14]. As shown in Fig. 1, the fundamental period of the core oscillation coincides with five focusing periods with a very good accuracy. We can also see in Fig. 1 that the core oscillation is almost dominated by the mismatch mode, and that the contribution from the periodic nature of focusing field is fairly small. Plotting test particle positions every five focusing periods, we successfully obtain the Poincaré surface of section plot shown in Fig. 2. In this figure, the test particle position divided by $R_{\max}\equiv R(0)$ is taken as the abscissa, and the strobe time is taken as $\tau=0 \bmod 5$. Figure 2 exhibits a striking resemblance with continuous focusing

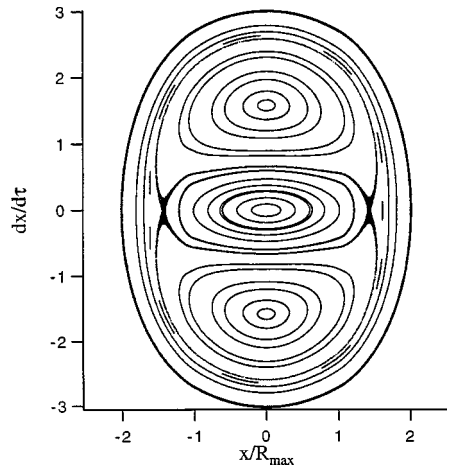

FIG. 2. Poincaré surface of section plot for a beam in a periodic solenoid channel. The same parameters as in Fig. 1 are adopted. The test particle positions are plotted every five focusing periods, taking the strobe time as $\tau=0 \bmod 5$.

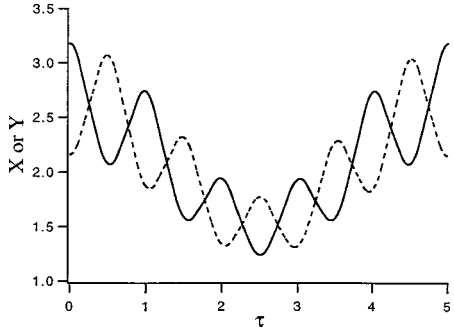

FIG. 3. Time evolution of the scaled beam envelope in a FODO channel (breathing oscillation case). The parameters are set to $\sigma_0=45°$, $\eta=0.5$, and $M_x=0.3$ to yield $\sigma_m=72°$. The solid and broken lines, respectively, represent the scaled beam half-width for the horizontal and vertical directions.

cases [2]. There is no smearing of the Poincaré plot as would occur if $\sigma_m/2\pi$ were irrational.

III. ALTERNATING-GRADIENT CHANNEL

A. Numerical method

This strategy is also applicable to the beams in channels without axial symmetry such as FODO channels. Assuming that the zero-current phase advance and emittance are the same in the horizontal and vertical directions, the envelope equations are given in terms of dimensionless variables as

$$\frac{d^2X}{d\tau^2}+\vartheta(\tau)X-\frac{2\Gamma}{X+Y}-\frac{1}{X^3}=0 \tag{7}$$

and

$$\frac{d^2Y}{d\tau^2}-\vartheta(\tau)Y-\frac{2\Gamma}{X+Y}-\frac{1}{Y^3}=0, \tag{8}$$

where X and Y are, respectively, the scaled beam half-width for the horizontal and vertical directions. The matched solution X_0 and Y_0 can be obtained numerically. The mismatch parameters for the horizontal and vertical directions can be defined as $M_x=[X(0)-X_0(0)]/X_0(0)$ and $M_y=[Y(0)-Y_0(0)]/Y_0(0)$, respectively. It should be noted that $X_0(0)$ and $Y_0(0)$, respectively, correspond to the maximum and minimum of the beam half-width of a matched beam since the origin of the coordinate τ is located at the center of a focusing quadrupole magnet.

It is to be noted that two types of mismatch mode oscillation can be excited in a FODO channel. One is the breathing mode oscillation which was also considered in Sec. II. The other is the quadrupole mode oscillation, where the oscillation for the horizontal and vertical directions are 180° out of phase. The frequency of the breathing mode oscillation can be obtained again by Eq. (4). The frequency of the quadrupole mode oscillation is given by

$$\sigma_m=\sqrt{1+3\eta^2+5\eta^2M_s^2}\,\sigma_0, \tag{9}$$

which is obtained in an analogous way with Eq. (4).

As we assume that there is no coupling between the horizontal and vertical motion except for the space-charge force,

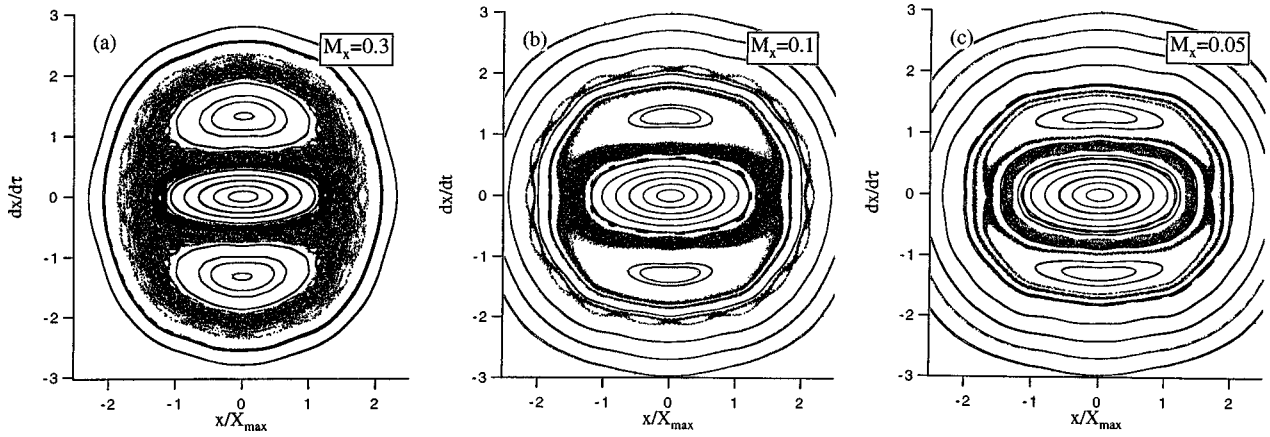

FIG. 4. Poincaré surface of section plots for beams with $\eta=0.5$. The cores executing breathing mode oscillation in FODO channels have been considered. Three different mismatches, i.e., $M_x=0.3$, $M_x=0.1$, and $M_x=0.05$, have been applied. The test particle positions are plotted every five focusing periods, taking the strobe time as $\tau=0 \bmod 5$. Zero current phase advances are set to (a) $\sigma_0=45°$, (b) $\sigma_0=45.3°$, and (c) $\sigma_0=45.4°$, respectively, to yield $\sigma_m=72°$.

the beam ellipse remains to be upright in real space. Furthermore, we only consider the test particles which have no angular momentum. Therefore, the motion of the test particles initially located on the horizontal or vertical plane is restricted on that plane.

Thus the equations of motion for the test particle initially located on the horizontal plane can be written [3,15] as

$$\frac{d^2x}{d\tau^2}+\vartheta(\tau)x-\frac{2\Gamma}{X(X+Y)}x=0 \quad (|x|\leqslant X), \tag{10}$$

and

$$\frac{d^2x}{d\tau^2}+\vartheta(\tau)x-\frac{2\Gamma}{x^2+|x|\sqrt{x^2+Y^2-X^2}}x=0 \quad (|x|>X). \tag{11}$$

B. Numerical results for breathing mode oscillation cases

First, we will consider the cases where breathing mode oscillation of a core is excited. Figure 3 shows an example in which we consider a FODO channel having $\sigma_0=45°$ and a 50% filling factor. The beam parameters are set to be $\eta=0.5$ and $M_x=0.3$. These parameters are determined to yield $\sigma_m=360/5=72°$ using an optimization code and Eq. (4). We can see in Fig. 3 that the modulation of core oscillation due to the periodic nature of the focusing field is much larger than in periodic solenoid cases. Plotting test particle positions every five focusing periods, we successfully obtain a Poincaré surface of section plot.

Fixing the tune depression as $\eta=0.5$, three different initial mismatches, i.e., $M_x=0.3$, $M_x=0.1$, and $M_x=0.05$, are considered in Fig. 4. In this figure, the particle position scaled by $X_{max}\equiv X(0)$ is taken as the abscissa, and the strobe time is taken as $\tau=0 \bmod 5$. Figure 4 exhibits strong chaoticity, which is a striking contrast to solenoid focusing cases.

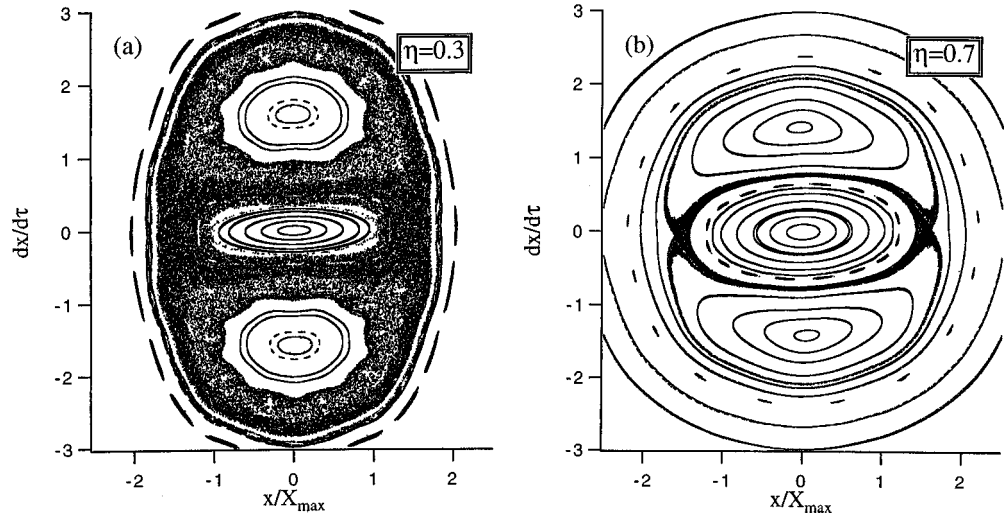

FIG. 5. Poincaré surface of section plots for beams with $M_x=0.3$. The cores executing breathing mode oscillation in FODO channels have been considered. Two different tune depressions, i.e., $\eta=0.3$ and 0.7, have been considered. The test particle positions are plotted every five focusing periods, taking the strobe time as $\tau=0 \bmod 5$. Zero current phase advances are set to (a) $\sigma_0=48°$ and (b) $\sigma_0=40.2°$, respectively, to yield $\sigma_m=72°$.

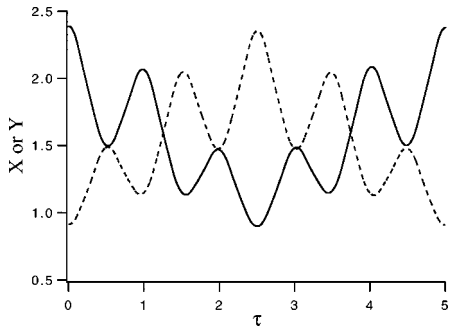

FIG. 6. Time evolution of the scaled beam envelope in a FODO channel (quadrupole oscillation case). The parameters are set to $\sigma_0=52.75°$, $\eta=0.5$, and $M_x=0.3$ to yield $\sigma_m=72°$. The solid and broken lines, respectively, represent the scaled beam half-width for the horizontal and vertical directions.

The chaotic region surrounds both the core and the 2:1 resonance islands, and such a kind of chaotic region is thought to enhance halo intensity. As such strong chaosity is observed only with higher beam density in solenoid focusing cases, it can be concluded that the global chaos is observed in wider parameter space in alternating-gradient focusing cases than in solenoid focusing cases. Actually, we have observed the global chaos even with a mismatch of 10% in the case of $\eta=0.5$, as shown in Fig. 4(b). As the degree of mismatch is decreased, some invariant curves are restored at a certain threshold and separate the chaotic region into several stochastic layers. As a result, the global chaos which contributes to the enhancement of the halo intensity disappears. We have found that the threshold exists between $M_x=0.05$ and 0.1 in the case of $\eta=0.5$. In fact, Fig. 4(c) shows that the particles initially located in the vicinity of the core are confined by an invariant curve and cannot escape to orbit around the 2:1 resonance islands in the case of 5% mismatch.

Figure 5 shows Poincaré surface of section plots for beams with lower and higher tune depressions, i.e., $\eta=0.3$ and 0.7, but the same initial mismatch, i.e., $M_x=0.3$. As shown in Fig. 5(a), the Poincaré plots for beams with higher beam density are similar to that for the $\eta=0.5$ case. Conversely, as can be clearly seen in Fig. 5(b), the results for the lower density cases exhibit a remarkable difference from the $\eta=0.5$ case. A sudden decrease of chaotic area is occurred at around $\eta=0.5\sim0.6$. Note here that, in spite of the decrease of chaosity, the global chaos which is expected to increase halo intensity is seen even in the low density case with $\eta=0.7$.

C. Numerical results for quadrupole mode oscillation cases

Second, we will consider the cases where quadrupole mode oscillation of a core is excited. Figure 6 shows the time evolution of a core executing a quadrupole mode oscillation. A FODO channel having $\sigma_0=52°$ and a 50% filling factor is considered, and the beam parameters are set to be $\eta=0.5$ and $M_x=0.3$. These parameters are determined to yield $\sigma_e=360/5=72°$ using an optimization code and Eq. (9).

The dependence of the phase space topology on the degree of mismatch is shown in Fig. 7, where three different initial mismatches, i.e., $M_x=0.3$, $M_x=0.1$, and $M_x=0.05$, are considered fixing the tune depression as $\eta=0.5$. The most interesting feature shown in Fig. 7 is the existence of two wide chaotic regions formed around the central core. One is the chaotic region surrounding the core and the 2:1 resonance islands, which is also seen in breathing oscillation cases. As readily seen in Fig. 7, the distance between the core boundary and the stable fixed points of the 2:1 resonance is shorter than in breathing oscillation cases. This results in a decrease of the chaotic area surrounding the 2:1 resonance islands. The other is the wide chaotic band surrounding the inner chaotic region, which is observed only in quadrupole oscillation cases. A closer look reveals that these two chaotic regions are separated by an invariant curve in all three cases in Fig. 7. Because of the existence of the invariant curve, the particles initially located in the vicinity of the core are confined into the inner chaotic region. Note here that, as shown in Fig. 7(c), these chaotic regions are observed even in the slightly mismatched case with 5% mismatch in contrast to breathing oscillation cases.

The density dependence of Poincaré plots is shown in Fig. 8, where two different tune depressions, i.e., $\eta=0.3$ and 0.7, are considered, fixing the mismatch factor as $M_x=0.3$. As

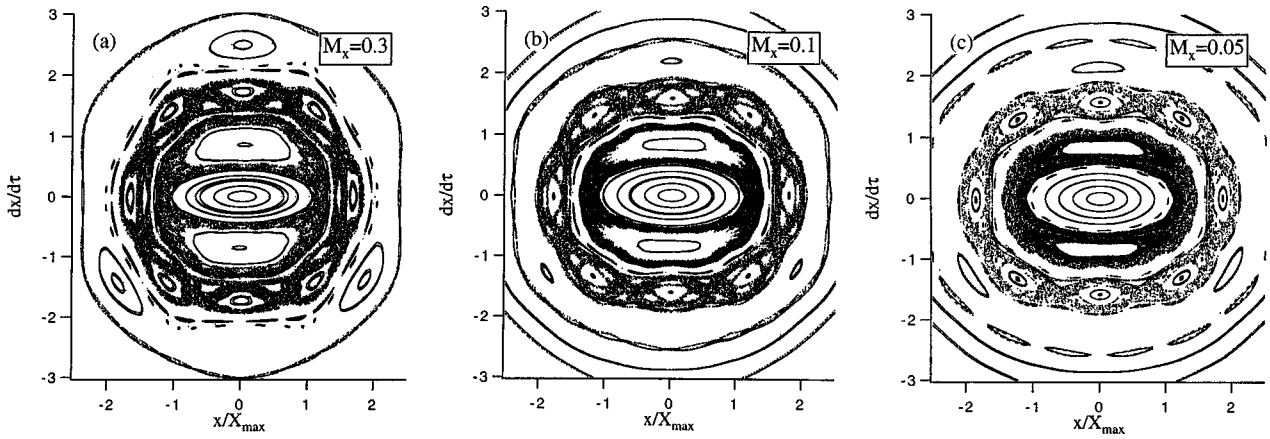

FIG. 7. Poincaré surface of section plots for beams with $\eta=0.5$. The cores executing quadrupole mode oscillation in FODO channels have been considered. Three different mismatches, i.e., $M_x=0.3$, $M_x=0.1$, and $M_x=0.05$ have been applied. The test particle positions are plotted every five focusing periods, taking the strobe time as $\tau=0 \bmod 5$. Zero current phase advances are set to (a) $\sigma_0=52.75°$, (b) $\sigma_0=54°$, and (c) $\sigma_0=54.25°$, respectively, to yield $\sigma_m=72°$.

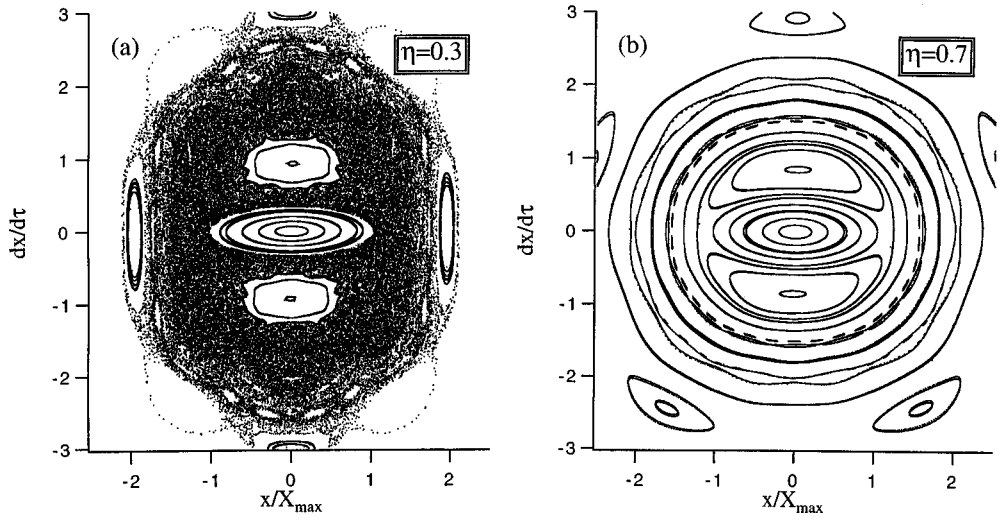

FIG. 8. Poincaré surface of section plots for beams with $M_x=0.3$. The cores executing quadrupole mode oscillation in FODO channels have been considered. Two different tune depressions, i.e., $\eta=0.3$ and 0.7, have been considered. The test particle positions are plotted every five focusing periods, taking the strobe time as $\tau=0 \bmod 5$. Zero current phase advances are set to (a) $\sigma_0=61.5°$ and (b) $\sigma_0=44.8°$, respectively, to yield $\sigma_m=72°$.

shown in Fig. 8(a), as the beam density is increased, the invariant curve separating the chaotic region into two chaotic regions is destroyed, and a large chaotic sea is formed. The threshold at which the invariant curve is destroyed is located between $\eta=0.4$ and 0.5 in the case of $M_x=0.3$. Conversely, as can be readily seen in Fig. 8(b), the chaotic region is not present in cases with lower beam density. The chaotic region disappears at around $\eta=0.5\sim0.6$.

IV. HALO EXTENT

In the usual particle-core analysis, test particles locked into the 2:1 resonance are considered to be halo particles. The oscillation amplitude of these particles is known to be self-limited due to the amplitude dependence of oscillation frequency. Thus, to estimate the maximum halo radius, we simply examine the maximum radius of the particle which is located on the separatrix of the 2:1 resonance island. In continuous focusing cases, the maximum radius can be easily obtained by making a Poincaré plot with the strobe time taken when the core radius is minimum. In that way, the maximum halo radius is found to be approximately twice as large as the maximum core radius [2].

However, the maximum halo extent in a periodic channel cannot be obtained generally in an analogous way. As an example, let us show a Poincaré plot in Fig. 9(a), where the strobe time is taken to be $\tau=2.5 \bmod 5$ and other parameters are set to be the same with Fig. 4(a). In Fig. 9(a), the 2:1 fixed points are located on the abscissa, and the core half-width is minimized. However, the width of the separatrix does not reach the maximum because the core half-width is too small at the strobe time due to strong external focusing force. In fact, it is easily seen that the separatrix width in Fig. 9(a) is smaller than that in Fig. 4(a). This means that halo width is not always maximized when the core width is at a minimum in periodic focusing cases. Tracking the particle

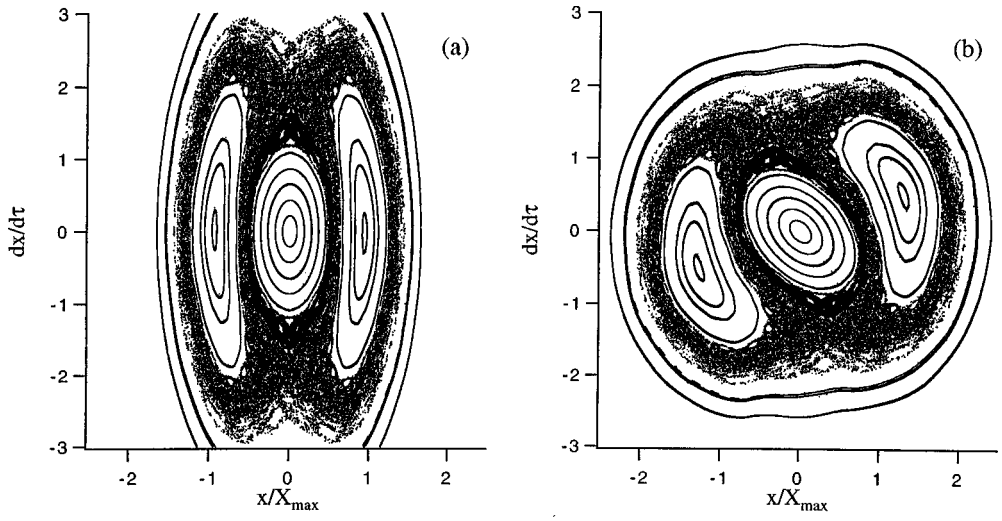

FIG. 9. Poincaré surface of section plots for a breathing beam in a FODO channel. The strobe times are taken as (a) $\tau=2.5 \bmod 5$ and (b) $\tau=2 \bmod 5$, respectively. Other parameters are taken to be the same as in Fig. 4(a).

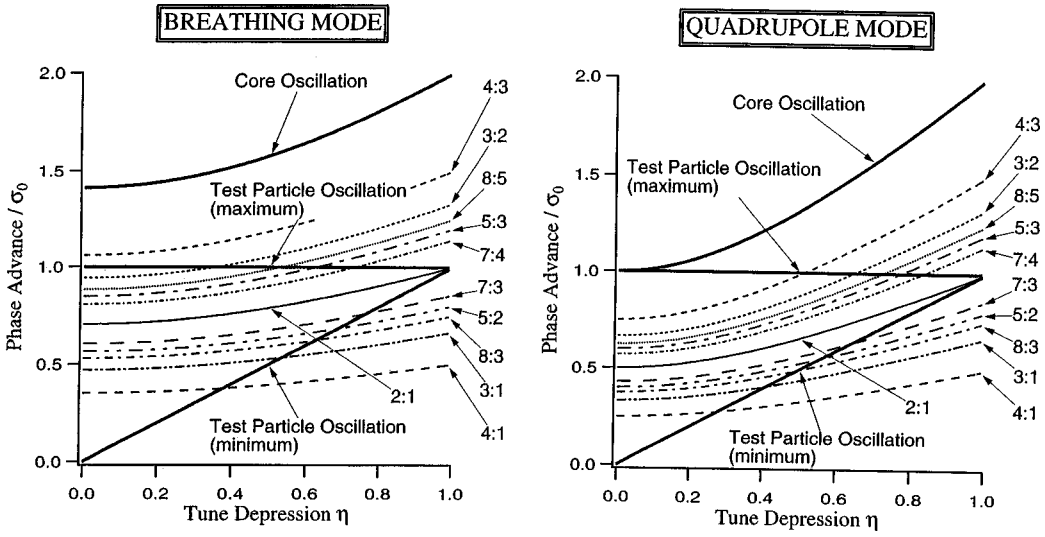

FIG. 10. Resonance lines of the 2:1 and higher order particle-core resonances in the weak mismatch limit. The resonance frequency scaled by the single particle zero-current betatron frequency is taken as the ordinate. The cores executing breathing and quadrupole mode oscillations are considered. The core frequency for those modes is calculated by Eqs. (4) and (9). The maximum and minimum betatron frequencies of the test particles are also shown.

which is initially located in the vicinity of the separatrix, we find that the halo width reaches a maximum at around $\tau = 2 \bmod 5$ or $\tau = 3 \bmod 5$ in this case. A Poincaré plot is shown in Fig. 9(b), where the strobe time is taken as $\tau = 2 \bmod 5$. We readily see in Fig. 9(b) that the maximum halo width is approximately twice as large as the maximum core width. This is roughly the same size as those in continuous focusing cases. Similar results are found in general for breathing oscillation cases in both periodic solenoid and FODO channels.

The results for quadrupole oscillation cases show some more complicated features. First, let us consider the case where the global chaos is not seen, as is the case in Fig. 8(b). In this case, we can consider only the particles locked into the 2:1 resonance as halo particles. It is readily seen that the maximum halo width is much smaller than in breathing oscillation cases, because the fixed points of the 2:1 resonance are located nearer to the core boundary. In fact, the typical halo width in this case is found to be about 1.2 times as large as the maximum core width. Second, we consider the case where the global chaos emerges, but it is divided by an invariant curve into two chaotic regions as is the case in Fig. 7. In this case, the maximum halo width is, again, found to be much smaller than in breathing oscillation cases, if we consider only the particles in the inner chaotic region as halo particles. Finally, as the beam density becomes higher than a certain threshold, the invariant curve is destroyed and two chaotic regions merge into one large chaotic sea, as is the case in Fig. 8(a). As the invariant curve disappears, the particle initially located in the inner chaotic region starts to diffuse, and this results in a sudden increase of halo extent. Thus the halo extent is density dependent in the case of the quadrupole mode oscillation. The halo width is roughly twice as large as the maximum core width in the case where the invariant curve is destroyed. This is roughly the same size as those in breathing oscillation cases.

V. DISCUSSION

As shown in the preceding sections, stronger chaosity is observed in alternating-gradient cases than in solenoid focusing cases. The strong core modulation due to the external focusing field in an alternating-gradient channel is thought to be a main cause of this difference. The phase advance of each test particle σ_t is amplitude dependent, and takes a value between $\eta\sigma_0$ and σ_0. As shown in Fig. 10, resonance lines of the 2:1 and higher order particle-core resonance exist in this range. Test particles whose betatron frequency is sufficiently near to the resonance frequency are trapped by the resonance. Furthermore, there must be resonance driven by the external focusing periodicity. That is, there exists resonance between the test particle oscillation and the external focusing periodicity which satisfy the conditions, $\sigma_t/2\pi = n/m$ and $\eta\sigma_0 < \sigma_t < \sigma_0$. Because the order of the *particle-structure resonance* is usually high, the effect of the resonance itself is expected to be small. However, the resonance overlap between the particle-structure resonance and particle-core resonance can modify the phase space topology, and result in global chaoticity. The effect of the particle-structure resonance is much stronger in an alternating-gradient channel because of the strong core modulation due to the external focusing force. That seems to be the reason why the strong chaoticity is observed in an alternating-gradient channel. The existence of the strong chaoticity suggests that the requirement on the degree of mismatch and beam intensity to suppress halo may be severer in alternating-gradient channels than in periodic solenoid channels.

Another interesting feature which has been found in this study is the difference of the phase space topology between breathing and quadrupole mode oscillation cases. In quadrupole oscillation cases, two chaotic regions are found with certain beam density, as shown in Fig. 7. The inner chaotic region surrounds the core and the 2:1 resonance islands. The outer chaotic band is formed around the inner chaotic region, which is observed only in quadrupole mode oscillation cases. The existence of the outer chaotic region suggests that certain higher order particle-core resonances has more importance than in breathing oscillation cases. As shown in Fig.

10, there are many particle-core resonance lines and each of them, more or less, affects the phase space topology. The degree of the influence on test particle motion is strongly dependent on the order of the resonance and the fixed point location. In general, the particle-core resonance has narrow width and hardly affects test particle motion if the fixed point locations are too near to the core boundary. Conversely, a resonance whose fixed points are located too far from the core cannot affect the motion of the test particles which are initially located in the vicinity of the core. As readily seen in Fig. 10, the resonance frequency of the 2:1 resonance is a little lower in quadrupole oscillation cases compared to breathing oscillation cases. Accordingly, the fixed point location of the resonance becomes nearer to the core boundary, and the island width is decreased. Instead, the fixed points of a resonance whose frequency is a little higher than the 2:1 resonance shift toward the core boundary. Then the effect of the resonance on test particle motion is increased. This seems to be why certain higher order resonances have more importance in quadrupole oscillation cases compared to breathing oscillation cases.

In this study, we have considered only cases where either the breathing or quadrupole mode oscillation is excited. However, the initial mismatch, in general, induces both modes of oscillation in an actual machine. The simultaneous excitation of both modes increases the density of the resonance lines. The resulting resonance overlap may cause stronger chaosity in wider parameter space. Finally, it should be noted that the technique we use in this study is also applicable to investigate halo formation in a circular machine, provided that the effect of the dispersion can be neglected [16].

VI. SUMMARY

We have shown a way of determining the fundamental frequency of stable core oscillation based on the smooth-approximation analysis. Using this technique, we carefully choose parameters to yield favorable core frequencies, which allows a Poincaré surface of section plot to be obtained for a mismatched beam in a periodic focusing channel. The plots for a periodic solenoid channel show a striking resemblance to those in continuous focusing cases. The focusing field periodicity does not play an important role in a periodic solenoid case. This is consistent with the results obtained in macroparticle simulations.

The same method is also applied to the beams in FODO channels, where both breathing and quadrupole modes of the core oscillation have been considered. Though some differences of the phase space topology are observed between breathing and quadrupole oscillation cases, stronger chaosity is found to exist in both cases in a wider parameter space. This suggests that the strong modulation of the core oscillation due to alternating-gradient focusing force affects the test particle stability and induces strong chaosity. The stronger chaosity is thought to cause an increase of halo intensity, and makes the conditions imposed to suppress halo intensity under a certain level more severe.

The halo extent is examined. It is found that the maximum halo width is about twice as large as the maximum core width in breathing mode oscillation cases in both periodic solenoid and FODO channels. In quadrupole mode oscillation cases, the halo width is density dependent, and ranges from 1.2 to 2 times as large as the maximum core width. In short, in spite of the significant difference of the phase space topology from the corresponding continuous situation, the maximum halo width in a periodic focusing channel is smaller than or comparable with that obtained in continuous focusing cases. This gives us a practical criterion for determining the bore radius of an accelerating structure in designing high-current ion accelerators.

ACKNOWLEDGMENTS

The author gratefully acknowledges helpful discussions with Dr. R. A. Jameson of LANL and Dr. S. Machida of KEK-Tanashi on several points in this paper. He also thanks Dr. M. Mizumoto and Dr. K. Hasegawa of JAERI for reading the manuscript and for making helpful suggestions.

[1] See, for example, M. Promé, in *Proceedings of the XVIII International Linac Conference*, edited by C. Hill and M. Vretenar (CERN, Geneva, 1996), p. 9.

[2] J. S. O'Connell, T. P. Wangler, R. S. Mills, and K. R. Crandall, in *Proceedings of the 1993 Particle Accelerator Conference*, edited by S. T. Corneliussen (IEEE, Piscataway, NJ, 1993), p. 3926; J. M. Lagniel, Nucl. Instrum. Methods Phys. Res. A **345**, 46 (1994); R. L. Gluckstern, Phys. Rev. Lett. **73**, 1247 (1994); A. Riabko, M. Ellison, X. Kang, S. Y. Lee, D. Li, J. Y. Liu, X. Pei, and L. Wang, Phys. Rev. E **51**, 3529 (1995); T. P. Wangler, R. W. Garnett, E. R. Gray, R. D. Ryne, and T. S. Wang, in *Proceedings of the XVIII International Linac Conference*, edited by C. Hill and M. Vretenar (CERN, Geneva, 1996), p. 372.

[3] J. M. Lagniel, Nucl. Instrum. Methods Phys. Res. A **345**, 405 (1994); Q. Qian, R. C. Davidson, and C. Chen, Phys. Rev. E **51**, R5216 (1995); Y. Fink, C. Chen, and W. P. Marable, *ibid.* **55**, 7557 (1997).

[4] I. M. Kapchinskij and V. V. Vladimirskij, in *Proceedings of International Conference for High Energy Accelerators* (CERN, Geneva, 1959), p. 274.

[5] A. J. Lichtenberg and M. A. Lieberman, *Regular and Chaotic Dynamics*, 2nd ed. (Springer-Verlag, New York, 1991), Chap. IV.

[6] R. A. Jameson, Los Alamos National Laboratory Report Nos. LA-UR-93-1209, 1993 (unpublished) and LA-UR-94-3753, 1994 (unpublished); H. Okamoto and M. Ikegami, Phys. Rev. E **55**, 4694 (1997).

[7] M. Ikegami and H. Okamoto, Jpn. J. Appl. Phys. **36**, 7028 (1997).

[8] J. M. Lagniel, in *Proceedings of the 1995 Particle Accelerator Conference* (IEEE, Piscataway, NJ, 1995), p. 3235.

[9] C. Chen and R. C. Davidson, Phys. Rev. E **49**, 5679 (1994); Phys. Rev. Lett. **72**, 2195 (1994); S. Y. Lee and A. Riabko, Phys. Rev. E **51**, 1609 (1995); Q. Qian and R. C. Davidson, *ibid.* **53**, 5349 (1996).

[10] M. Reiser, *Theory and Design of Charged Particle Beams* (Wiley, New York, 1994), Chap. IV.

[11] T. Suzuki, KEK Report No. KEK-74-6, 1974 (unpublished).

[12] The assumption of rational $\sigma_m/2\pi$ is not a real restriction; that is, there are always rational numbers arbitrarily close to any real number, and hence the deviation of the envelope evolution for rational $\sigma_m/2\pi$ from the real orbit can be made arbitrarily small in principle. The commensurable frequency corresponds to a kind of structure resonance conditions. However, the solution of the envelope equation is known to be stable with the reasonable choice of parameters. Thus, in the parameter space of our interest, namely, $M \leqslant 0.3$ and $\sigma_0 < 90°$, we do not need to care about the envelope instability.

[13] E. Forest and R. D. Ruth, Physica D **43**, 105 (1990); H. Yoshida, Phys. Lett. A **150**, 262 (1990).

[14] Though, Eq. (4) gives us a rough estimate of the core frequency, the accuracy is not sufficient for our purpose. To improve the accuracy, we employ an optimization code with the result obtained from Eq. (4) as the starting point. Employing the optimization procedure, the fundamental period can be estimated as accurately as in usual particle-core analysis.

[15] See for example, O. D. Kellog, *Foundation of Potential Theory* (Ungar, New York, 1953), Chap. VII.

[16] S. Machida and M. Ikegami, in *Workshop on Space Charge Physics in High Intensity Hadron Rings, Shelter Island, 1998,* edited by A. U. Luccio and W. T. Weng, AIP Conf. Proc. No. 448 (AIP, Woodbury, NY, 1998), p. 73.